

Article

A Cooperative Control Method for Wide-Range Maneuvering of Autonomous Aerial Refueling Controllable Drogue

Jinxin Bai and Zhongjie Meng * 

School of Astronautics, Northwestern Polytechnical University, Xi'an 710072, China;
2021100518@mail.nwpu.edu.cn

* Correspondence: mengzhongjie@nwpu.edu.cn

Abstract: In the realm of autonomous aerial refueling missions for unmanned aerial vehicles (UAVs), the controllable drogue represents a novel approach that significantly enhances both the safety and efficiency of aerial refueling operations. This paper delves into the issue of wide-range maneuverability control for the controllable drogue. Initially, a dynamic model for the variable-length hose–drogue system is presented. Based on this, a cooperative control framework that synergistically utilizes both the hose and the drogue is designed to achieve wide-range maneuverability of the drogue. To address the delay in hose retrieval and release, an open-loop control strategy based on neural networks is proposed. Furthermore, a closed-loop control method utilizing fuzzy approximation and adaptive error estimation is designed to tackle the challenges posed by modeling inaccuracies and uncertainties in aerodynamic parameters. Comparative simulation results show that the proposed control strategy can make the drogue maneuvering range reach more than 6 m. And it can accurately track the time-varying trajectory under the influence of model uncertainty and wind disturbance with an error of less than 0.1 m throughout. This method provides an effective means for achieving wide-range maneuverability control of the controllable drogue in autonomous aerial refueling missions.

Keywords: unmanned aerial vehicle; autonomous aerial refueling; controllable drogue; cooperative control; adaptive fuzzy control



Citation: Bai, J.; Meng, Z.

A Cooperative Control Method for Wide-Range Maneuvering of Autonomous Aerial Refueling Controllable Drogue. *Aerospace* **2024**, *11*, 845. <https://doi.org/10.3390/aerospace11100845>

Received: 21 August 2024

Revised: 7 October 2024

Accepted: 10 October 2024

Published: 14 October 2024



Copyright: © 2024 by the authors. Licensee MDPI, Basel, Switzerland. This article is an open access article distributed under the terms and conditions of the Creative Commons Attribution (CC BY) license (<https://creativecommons.org/licenses/by/4.0/>).

1. Introduction

In recent years, unmanned aerial vehicles (UAV) have developed rapidly and have been widely used in many fields [1–3]. The duration of flight has always been a major issue limiting its application. Autonomous Aerial Refueling (AAR) technology can effectively improve the endurance of UAVs and has attracted widespread attention [4]. In this area, a novel concept of a controllable drogue has been proposed recently [5,6]. Through actuators on the drogue, it can actively maneuver and dock with the refueling plug. Compared with the traditional aerial refueling methods, a controllable drogue can significantly improve the safety and efficiency of the AAR mission [7]. However, due to the complex flow field around the drogue [8,9] and the large uncertainties in the model of the refueling hose–drogue system, stabilizing and maneuvering the controllable drogue is very difficult.

In terms of dynamic modeling of the hose–drogue system, Williamson et al. [5] proposed a dynamic model for the hose–drogue system, in which the refueling hose is assumed to be a straight rod and the bending characteristics are ignored. Subsequently, in [10] by Ro et al., the hose was established as a multi-link model consisting of many straight links and frictionless joints. Based on this model, the hose bending recovery force and the wind interference were both considered in [11] by Wang et al. Furthermore, Paniagua et al. [9] considered the hose as a continuum and introduced a micro-element method to analyze the vibration characteristics of the hose. Similarly, Clifton et al. [12] also adopted the continuum assumption and derived the dynamics model of the towing system using the catenary theory. The release and retrieval of the hose have been neglected in the above studies.

Kamman et al. [13] investigated the dynamics of the cable retrieve/release process based on the multi-link model for an underwater towing system. This theory is also applicable to the AAR mission. Cheng et al. [14] considered the length of the first link of the hose to be variable based on the multi-link model.

In terms of control of the hose–drogue system, Williamson et al. [5] linearized the hose–drogue system model and used a linear quadratic regulator to realize stable control of the drogue. Su's team designed a trajectory tracking controller that combines high-order sliding mode observers and dynamic surface control [15]. Subsequently, in [16], an estimator-based minimal learning parameter neural network is used to accurately reconstitute the disturbances and uncertainties. Liu et al. [17–19] modeled the system using partial differential equations and achieved vibration control of the hose based on Lyapunov's direct method. Song et al. [20] designed a trajectory tracking control algorithm based on an improved extended state observer, solving the peaking issue. Furthermore, several studies in unrelated domains, including UAV control, also concentrate on model uncertainty, such as fuzzy systems [21] and neural networks [22]. In [23], an unknown input observer is employed to isolate the unknown time-varying delays in the state estimation process. Bianchi [24] makes use of high-order sliding mode estimators to estimate the perturbations that can be canceled by the control. Existing control algorithms for controllable drogue mostly focus on problems such as model inaccuracy and generally ignore the problem of aerodynamic parameter uncertainty. For this problem, the available methods include the Nussbaum function [25,26], adaptive estimation [27] and other methods. In this paper, the aerodynamic parameters and other model uncertainties are combined into one item and approximated using an adaptive fuzzy system.

Most of the current research focuses on the autonomous control of the controllable drogue. However, the maneuvering range is limited by relying solely on the drogue. Therefore, a cooperative control algorithm that comprehensively uses the hose retrieve/release device and drogue actuators is established. The main contributions of this paper are as follows:

- (1) Unlike the current methods that solely rely on the drogue actuator for maneuver control, this paper constructs a cooperative maneuver control framework that leverages open-loop control of the hose and closed-loop control of the drogue. This integration enables autonomous aerial refueling with wide-range maneuverability for UAVs.
- (2) The hose retraction and extension processes are subject to latency and error accumulation, which impedes the precise execution of closed-loop control. Existing research overlooks these issues. This paper introduces an open-loop control method for the hose based on neural networks, ensuring rapid convergence to the desired length.
- (3) Addressing the issues of model uncertainty and time-varying aerodynamic parameters in the drogue closed-loop control, this paper employs fuzzy systems to approximate the uncertain elements. Adaptive estimation of the approximation errors further enhances the control accuracy.

The rest of this paper is organized as follows. A complete refueling hose–drogue dynamic model is established in Section 2. A trajectory-tracking control method is proposed in Section 3, including a neural network approximator and an adaptive fuzzy controller. Section 4 verifies the controller performance using simulation experiments. Finally, the conclusion is drawn in Section 5.

2. Hose–Drogue System Dynamic Modeling

The dynamic model for the controllable drogue in the AAR mission includes the hose model and the drogue model. Considering the release and retrieval process, a recursion dynamic model of the refueling hose is established first. Then, the dynamic positioning model and the attitude dynamic model for the refueling drogue are proposed.

2.1. Recursive Dynamic Model of the Hose

In the dynamic model, the refueling hose is made to consist of a finite number of cylindrically shaped rigid links [10]. Two adjacent links are connected by a frictionless

spherical joint. The masses and loads of links are concentrated on joints. The coordinate systems are defined as follows: $Oxyz$ represents the inertial coordinate system. $O_vx_vy_vz_v$ represents the trajectory coordinate system of the refueling pod attached to the refueling tanker, with its origin O_v located at the hose tow-point. O_vx_v is pointed forward along the trajectory, O_vy_v is perpendicular to the plumb plane pointing to the right, and O_vz_v is directed to make $O_vx_vy_vz_v$ a right-hand coordinate system. $O_{hi}x_{hi}y_{hi}z_{hi}$ represents the hose coordinate system attached to the i^{th} link, with its origin O_{hi} located at the joint i . $O_{hi}x_{hi}$ points to the joint $i - 1$ along the rigid link, $O_{hi}y_{hi}$ is perpendicular to the plumb plane pointing to the right. $O_dx_dy_dz_d$ is the drogue body coordinate system. The origin O_d is located at the centroid of the drogue. O_dx_d is along the longitudinal axis of the drogue pointing to the hose side, O_dz_d is in the plane of symmetry of the drogue, and perpendicular to O_dx_d . All coordinate systems are shown in Figure 1.

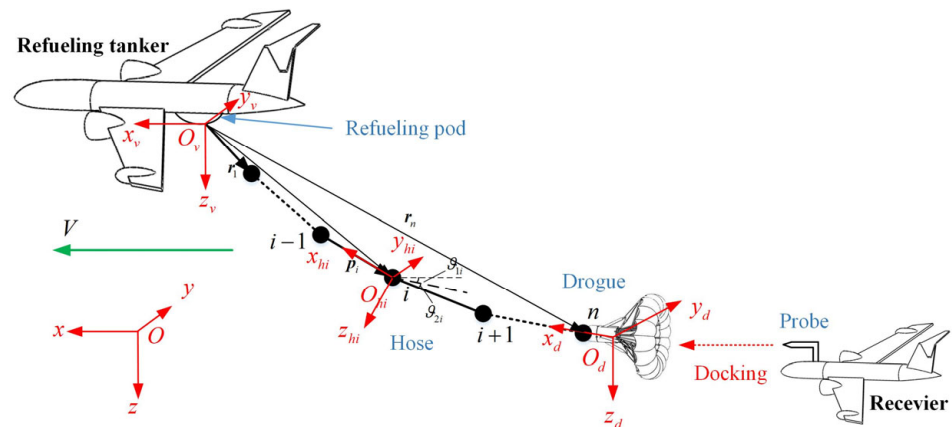


Figure 1. Schematic diagram of the hose–drogue system in the AAR mission.

In the initial state, every link has the same length of l_0 . During the hose length changes, it is assumed that only the length of the first link l_1 changes, and the rest remain unchanged. When the reel equipped on the tanker drives the hose to retrieve, the length of the first link decreases. When it is reduced to a certain extent, the first and second links are merged into a new first link, and the number of joints is reduced by one. The same goes for the hose release process. In this way, a wide range of length variations are achieved. As is shown in Equation (1), where n is the number of links, and v_{rec} and v_{rel} are the adjustment parameters when the hose is retrieved and released, respectively.

$$n = \begin{cases} n - 1, & l_1 < v_{rec}l_0 \\ n + 1, & l_1 > v_{rel}l_0 + l_0 \end{cases} \quad (1)$$

In Figure 1, r_i represents the position vector from the hose tow-point to joint i in $O_vx_vy_vz_v$, and p_i represents the position vector from joint $i - 1$ to joint i . Then,

$$r_i = r_{i-1} + p_i \quad (2)$$

where $p_i = l_i n_i$, l_i represents the length of the i th link. n_i represents the direction vector of the i th link. A set of azimuth angles, ϑ_{1i} and ϑ_{2i} , are used to represent the vector of the i th link and are in the vertical and lateral plane, respectively, as shown in Equation (3).

$$p_i = l_i [-\cos \vartheta_{1i} \cos \vartheta_{2i}, -\sin \vartheta_{2i}, \sin \vartheta_{1i} \cos \vartheta_{2i}] \quad (3)$$

Setting t_i represents the tension on the i th link. $Q_i = G_i + D_i + R_i$ denote forces acting on joint i except the hose tension, where G_i is the gravity, D_i is the aerodynamic force and R_i is the hose bending recovery force, whose formulas are all given in [11].

Referring to [15], the recursive dynamics of the hose are modeled as:

$$\ddot{\theta}_{ji} = \mathbf{p}_{i,\theta_{ji}} \cdot \left[\begin{array}{c} \mathbf{a}_i - \mathbf{a}_{i-1} - \mathbf{p}_{i,l} \ddot{l}_i - \dot{\mathbf{p}}_{i,l} \dot{l}_i - \sum_{j=1}^2 \dot{\mathbf{p}}_{i,\theta_{ji}} \dot{\theta}_{ji} \\ -\boldsymbol{\alpha}_i \times \mathbf{p}_i - \boldsymbol{\omega}_i \times \dot{\mathbf{p}}_i \end{array} \right] / (\mathbf{p}_{i,\theta_{ji}} \cdot \mathbf{p}_{i,\theta_{ji}}); i = 1, \dots, n; j = 1, 2 \quad (4)$$

where $p_{i,b} = \partial p_i / \partial b, b = l, \theta_{1i}, \theta_{2i}$, while $\mathbf{a}_i = (\mathbf{Q}_i + \mathbf{t}_i - \mathbf{t}_{i+1}) / m_i$ is the acceleration of joint i . Given the accelerations, the position vector and their derivatives of each link, the second derivatives of every azimuth angle can be calculated by Equation (4).

According to Equation (3), we have $\mathbf{p}_i \cdot \mathbf{p}_i = l_i^2$. After finding the second-order derivative and combining it with the joint acceleration formula, the recursive formula for the tension magnitude can be obtained as:

$$\begin{aligned} & -(\mathbf{n}_{i-1} \cdot \mathbf{n}_i) t_{i-1} / m_{i-1} - (\mathbf{n}_{i+1} \cdot \mathbf{n}_i) t_{i+1} / m_i + (1/m_{i-1} + 1/m_i) t_i \\ & = \ddot{l}_i + (\mathbf{Q}_{i-1} / m_{i-1} - \mathbf{Q}_i / m_i) \cdot \mathbf{n}_i + \left[\dot{l}_i^2 - ((v_i - v_{i-1})^2) \right] \end{aligned} \quad (5)$$

where v_i represents the velocity of joint i , and \dot{l}_i and \ddot{l}_i represent the first- and second-order derivative of the link length l_i , respectively.

2.2. Dynamic Model of the Controllable Drogue

The controllable drogue structure is shown in Figure 2. The drogue body is connected with four fixed struts and four maneuverable struts at the end. The ends of the struts are attached to the flexible canopy. Fixed struts are attached to the inner edge of the canopy, while maneuverable struts are attached to the outer edge. The mechanism of control force generation involves variations of the strut angle changing the shape and area of the canopy, thereby changing the aerodynamic force in the corresponding direction. Four pairs of struts are evenly distributed around the canopy and placed perpendicular to each other. This means that changing the angle of the four pairs of struts simultaneously can generate control force in two orthogonal directions. The vector of the strut angle is written as $\mathbf{u}_{act} = [u_1, u_2, u_3, u_4]^T$.

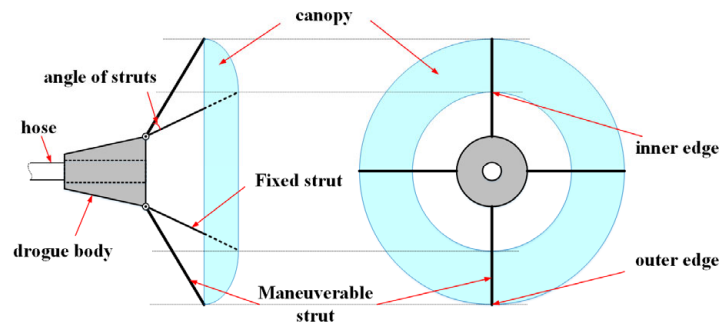


Figure 2. Side view (left) and front view (right) of the controllable drogue.

The aerodynamic force and moment of the drogue can be described as:

$$\begin{cases} D_{drogue} = qSC_{Ddro} = qS \left[C_{Ddro}^u \mathbf{u}_{act} + C_{Ddro}^{\alpha, \beta}(\alpha, \beta) \right] \\ M_{drogue} = qSLC_{Mdro} = qSL \left[C_{Mdro}^u \mathbf{u}_{act} + C_{Mdro}^{\alpha, \beta}(\alpha, \beta) \right] \end{cases} \quad (6)$$

where $q = 0.5\rho v_{i/a}^2$ represents the drogue's dynamic pressure, and $v_{i/a}$ represents the drogue velocity. S and L are the drogue's characteristic area and length, respectively. $C_{Ddro}^u, C_{Ddro}^{\alpha, \beta}(\alpha, \beta)$ are the aerodynamic force parameters of the drogue, and $C_{Mdro}^u, C_{Mdro}^{\alpha, \beta}(\alpha, \beta)$ are the aerodynamic moment parameters. α, β are the angle of attack and sideslip of the drogue, respectively.

For the convenience of description, unless otherwise specified, the position x in this paper refers to the position in the refueling pod track coordinate system. The dynamic model of the last joint is used to describe the drogue motion:

$$\ddot{x}_n = (G_n + D_n + D_{\text{drogue}} + R_n + t_n) / m_n \tag{7}$$

Unlike other joints, the aerodynamic force of the last joint includes the dynamic force of the last link D_n and the drogue D_{drogue} .

In addition to the position dynamics of the drogue, its attitude also needs to be considered. Settings ϕ, θ and ψ represent the roll angle, the pitch angle and the yaw angle. The drogue’s attitude kinematic equations are as follows [28]:

$$\dot{\Omega} = H(\Omega)\omega \tag{8}$$

where $\Omega = [\phi, \theta, \psi]^T$ represents the drogue attitude angle vector. $\omega = [\omega_x, \omega_y, \omega_z]^T$ represents the drogue angular velocity vector. Matrix H is as follows:

$$H(\Omega) = \begin{bmatrix} \cos(\theta) & 0 & \sin(\theta) \\ \tan(\phi) \sin(\theta) & 1 & -\tan(\phi) \cos(\theta) \\ -\sin(\theta) / \cos(\phi) & 0 & \cos(\theta) / \cos(\phi) \end{bmatrix}$$

The drogue’s attitude dynamic equations are as follows [28]:

$$I\dot{\omega} + \omega \times I\omega = M_{\text{drogue}} + M_t + M_R + M_n \tag{9}$$

where $I = \text{diag}(I_x, I_y, I_z)$ is the three-axis rotational moment of inertia of the drogue. M_n is the twisting moment of the hose and is assumed to be $M_n = -100\varphi - 10\omega_x$. $M_t = t \times s_d$ is the hose tension moment acting on the drogue, and $M_R = R_n \times s_d$ is the hose bending recovery moment. $s_d = \Gamma(\Omega)[-s, 0, 0]^T$ is the position vector from joint n to the drogue centroid, where s is the distance between these two points. $\Gamma(\Omega)$ is the transformation matrix from the drogue body coordinate system to the inertia coordinate system.

2.3. Dynamic Model of Refueling Hose–Drogue System

Combining the hose recursive dynamic model and the drogue position/attitude dynamic models, the complete refueling hose–drogue dynamic model can be formed as shown in Equation (10).

$$\left\{ \begin{array}{l} \ddot{\vartheta}_{j1} = \frac{p_{1,\vartheta_{j1}}}{(p_{1,\vartheta_{j1}} \cdot p_{1,\vartheta_{j1}})} \cdot \left[\begin{array}{l} (Q_1 + t_1 - t_2) / m_1 - \sum_{j=1}^2 \dot{p}_{1,\vartheta_{j1}} \dot{\vartheta}_{j1} \\ -\alpha_1 \times p_1 - \omega_1 \times \dot{p}_1 - p_{1,l} \ddot{l}_1 - \dot{p}_{1,l} \dot{l}_1 \end{array} \right] \\ \dots\dots \\ \ddot{\vartheta}_{j,n-1} = \frac{p_{n-1,\vartheta_{j,n-1}}}{(p_{n-1,\vartheta_{j,n-1}} \cdot p_{n-1,\vartheta_{j,n-1}})} \cdot \left[\begin{array}{l} (Q_{n-1} + t_{n-1} - t_n) / m_{n-1} - (Q_{n-2} + t_{n-2} - t_{n-1}) / m_{n-2} \\ -\sum_{j=1}^2 \dot{p}_{n-1,\vartheta_{j,n-1}} \dot{\vartheta}_{j,n-1} - \alpha_{n-1} \times p_{n-1} - \omega_{n-1} \times \dot{p}_{n-1} \end{array} \right] \\ \ddot{x}_n = (G_n + D_n + D_{\text{drogue}} + R_n + t_n) / m_n \\ \dot{\Omega} = H(\Omega)\omega \\ I\dot{\omega} + \omega \times I\omega = M_{\text{drogue}} + M_t + M_R + M_n \end{array} \right. \tag{10}$$

The purpose of this paper is to maneuver the drogue to the desired position while maintaining a stable attitude. There are two possible methods for solving this problem. One is to use the actuator to control the attitude, and then take the attitude as a virtual control quantity to control the position. The other is to control the position directly. In the actual AAR mission, hoses must transfer fuel as well as provide power and signal transmission. As a result, the diameter and rigidity of the refueling hose are large, and the attitude of the

drogue does not change significantly due to the change in the aerodynamic moment. The tension moment and the hose recovery moment will ensure the drogue attitude is always constrained by the azimuth of the hose. Therefore, the second method is more effective and is used in this paper.

However, the direct position control method requires the controller to be able to offset the influence of the attitude change on the drogue, which creates difficulties in the controller design. Furthermore, the influence of the first $n - 1$ links of the hose on the drogue position equations is mainly concentrated on the hose tension and hose bending recovery force. This information cannot be accurately measured in the actual AAR mission, which increases the difficulty greatly.

3. Refueling Drogue Trajectory Tracking Controller Designing

Figure 3 shows the cooperative controller with comprehensive utilization of hose retrieval/release and drogue actuators, where x_d, y_d, z_d are the instruction of the drogue position. L and u_{act} are the output of the hose’s receiving/releasing device and the drogue struts, respectively. In order to achieve the large-scale and all-around maneuvering of the drogue, all three directions of x, y, z need to be controlled.

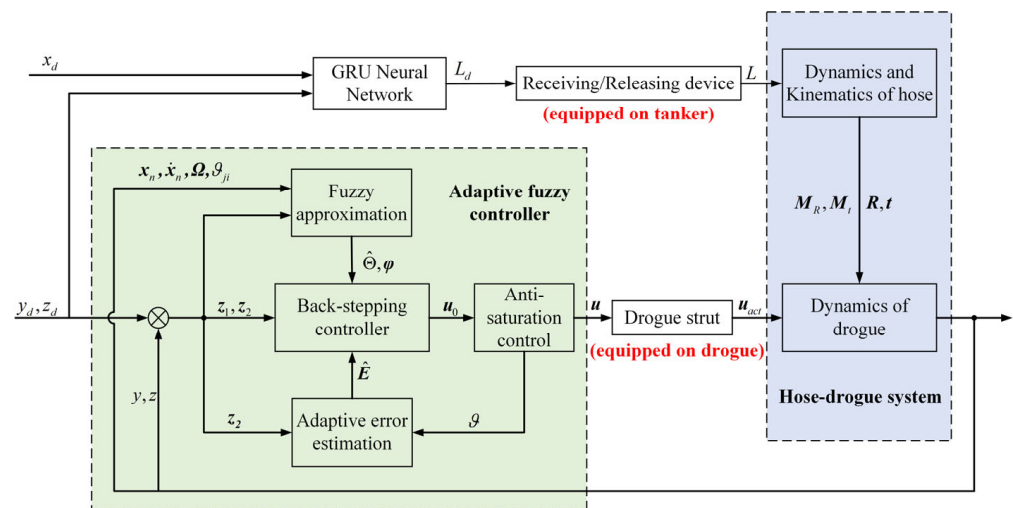


Figure 3. Cooperative control method for the controllable drogue.

The autonomous control of the drogue studied in this paper is realized by the variation in the canopy area in four directions. It is assumed that the sum of the areas of the canopy remains constant during the control process, which results in the drogue being unable to generate significant aerodynamic forces in the x direction. Therefore, maneuvering in this direction is realized by hose retrieval and release. Using a Gated Recurrent Unit (GRU) neural network to approximate the hose catenary model, the hose length is calculated online according to the desired drogue position. Maneuvering in other directions is realized by drogue actuators. The control inputs are angles of struts. A fuzzy approximator, whose parameters are updated adaptively, is used to approximate the model uncertainty terms and disturbance. Considering the controller saturation problem, a fuzzy-based anti-saturation controller is designed. Moreover, adaptive error estimation is used to estimate and compensate for the upper bound error of the two fuzzy systems.

3.1. Hose Retrieve/Release Controller Based on GRU Neural Network

The refueling pod’s motor is in charge of hose retrieval/release. Compared to the closed-loop control, the open-loop control procedure does not include a feedback mechanism, which is theoretically finished quickly and can ensure rapid convergence. In practice, the control rate of the hose is influenced by hose damping, reel power, and other variables, but it is always faster than closed-loop control. Furthermore, closed-loop control neces-

sitates real-time hose length measurements as well as an extremely fast retrieve/release response. The large mass and inertia of the refueling hose will cause a large accumulation of errors, making accurate control difficult. As a result, the open loop control strategy is used by the hose's retrieve and release controller.

During the flight task, the hose assumes a special catenary shape. A GRU neural network is then used to approximate the catenary model, which is used to characterize the relationship between the hose length and the position of the drogue under certain flight conditions, including the flight speed, hose mass and drogue mass. Figure 4 (left) depicts the GRU's basic structure. To obtain sufficient data, given the flight conditions and the hose length, the equilibrium position of the drogue can be calculated by the dynamic model (for real flight tasks, the equilibrium position can be obtained using the wind tunnel blow test). After that, using flight conditions and drogue equilibrium positions as inputs and the hose length as the output, the GRU can be trained offline. The training process and GRU parameters are as follows:

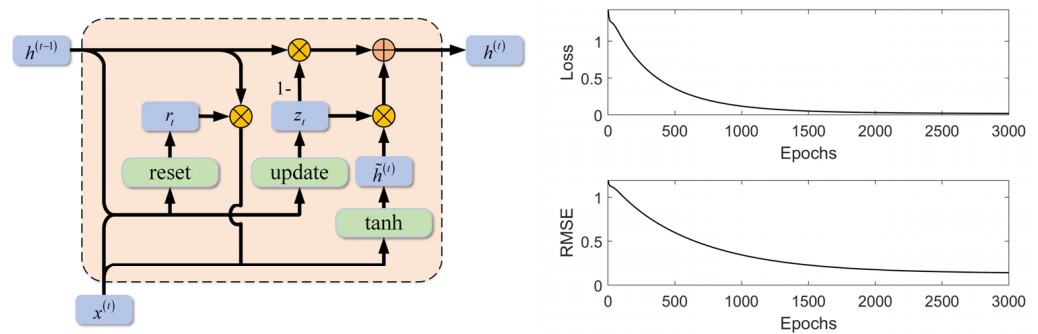


Figure 4. Structure of GRU neural network (left) and training process (right).

Step 1: Preprocess the data, including normalization and partitioning of training sets and test sets.

Step 2: Define a GRU model, with input dimension 4 and output dimension 3. The number of layers in the model is 3 and the number of hidden units is 100.

Step 3: Train the GRU model. Set the maximum number of iterations to 200, the initial learning rate to 0.005, and the learning rate decline factor to 0.5.

Step 4: Use the trained GRUs to make predictions and plot the curve of the loss function. Figure 4 (right) depicts the RMSE and loss during the training process, both of which converge near zero.

It is worth noting that because the hose retrieve/release control is open-loop, its response characteristics are faster than the drogue actuator closed-loop control. Therefore, it is reasonable that the change in hose length does not have a significant effect on the y and z direction control of the drogue. Furthermore, under the influence of factors such as actuator error, sensor error, wind interference, etc., the hose's retrieve/release control may exhibit errors for its open-looped characteristics. Because the two positions of y, z are controlled independently by an adaptive fuzzy controller, errors in these two directions are small. As a result, errors exist primarily in the direction of x . In an AAR mission, x is the docking direction between the drogue and the receiver, with far lower accuracy requirements than the other two directions. As a result, the open-loop hose retrieve/release control strategy used in this paper is feasible.

3.2. Strut Angles Controller Based on Adaptive Fuzzy Method

At present, most studies regard attitude as the inner loop variable of position. However, for the controllable drogue studied in this paper, its supporting refueling hose contains power lines, signal lines, etc. This results in a large diameter and stiffness. Therefore, according to the theoretical analysis and the experimental phenomenon of the relevant wind tunnel test conducted by the author, this paper directly believes that the attitude of the

drogue changes with the shape of the hose, that is, the drogue position is directly controlled by the drogue actuators. For the controllable drogue studied in this paper, struts in opposite directions generate aerodynamic force in the same direction. Then, four pairs of struts will generate two orthogonal directions of control force. Therefore, in this section, two pairs of opposite strut angles are combined into one, which generates the control force in the corresponding direction together, i.e.,

$$\mathbf{u} = [u_y, u_z]^T = [u_1 - u_3, u_2 - u_4]^T \tag{11}$$

For the directions of y and z , an adaptive fuzzy controller is designed in this section. Therefore, in order to facilitate the analysis and controller design, the drogue’s dynamic positioning model is rewritten as follows:

$$\begin{cases} \dot{\chi}_1 = \chi_2 \\ \dot{\chi}_2 = f_0 + f_1(x_n, \dot{x}_n, \Omega, \vartheta_{ji}) + g(\dot{x}_n, \Omega)\mathbf{u} \end{cases} \tag{12}$$

where, $f_0 = G_n/m_n$, $f_1(x_n, \dot{x}_n, \Omega, \vartheta_{ji}) = (D_n + R_n + t_n + qS C_{Ddro}^{\alpha, \beta}(\alpha, \beta))/m_n$, $g(\dot{x}_n, \Omega) = qS C_{Ddro}^u$, $\chi_1 = [y, z]^T$, and $\chi_2 = [\dot{y}, \dot{z}]^T$. f_0 denotes known items in the dynamic model, i.e., gravity. The hose’s aerodynamic force, bending recovery force, hose tension, and items in the drogue’s aerodynamic force that are not related to the control variable \mathbf{u} are all contained in f_1 . These items cannot be accurately measured in real-time, which are classified as model uncertainties. The items that are related to the control variable are denoted by g . The drogue’s aerodynamic force will change with the complex flow field because the drogue canopy is flexible. Therefore, g is also thought to be unknown. It is assumed that g is invertible and has the upper bound of g_0 , and its first-order derivative has the upper bound of g_d .

The error vector is defined as $z_1 = \chi_1 - \chi_d$, and then, $\dot{z}_1 = \chi_2 - \dot{\chi}_d$.

The Lyapunov function is defined as:

$$V_1 = \frac{1}{2} z_1^T z_1 \tag{13}$$

The virtual control law is designed as:

$$\alpha_1 = -K_1 z_1 + \dot{\chi}_d \tag{14}$$

where the matrix $K_1 = \text{diag}(k_{11}, k_{12})$ is designed as positive-definite to ensure that $\dot{V}_1 = z_1^T \dot{z}_1 = -z_1^T K_1 z_1$ is negative-definite.

For the second-order subsystem, define the error vector $z_2 = \chi_2 - \alpha_1$, and then $\dot{z}_2 = g[g^{-1}(f_0 + f_1 - \dot{\alpha}_1) + \mathbf{u}]$, where $g^{-1}(f_0 + f_1 - \dot{\alpha}_1)$ is unknown. A fuzzy system is used to approximate it. According to the universal approximation theorem [29], singleton fuzzification, product inference and central weighted defuzzification methods are used. Then, a fuzzy system is constructed to approximate the uncertain terms:

$$\theta_1^T \varphi_1(X) + \varepsilon_1(X) = g^{-1}(f_0 + f_1 - \dot{\alpha}_1) \tag{15}$$

where $X = [\chi_1, \chi_2, \Omega, \vartheta_{ji}, \dot{\alpha}_1]$ is the fuzzy system input. Then, $\dot{z}_2 = g[\theta_1^T \varphi_1(X) + \varepsilon_1(X) + \mathbf{u}]$. The control law is designed as follows:

$$\mathbf{u}_0 = [u_{y0}, u_{z0}]^T = -z_1 - K_2 z_2 - \frac{\hat{\Theta}_1 z_2 \varphi_1^T \varphi_1}{2\sigma_1^2} - \hat{E}_1 \text{sgn}(z_2) + g_d g_0^{-2} z_2 \tag{16}$$

where $\Theta_1 = \|\theta_1\|^2$, which is bounded. And \hat{E}_1 represents the estimate of the upper bound of $\varepsilon_1(X)$. $\sigma_1^2 > 0$ is the control parameter to be designed. $K_2 = \text{diag}(k_{21}, k_{22})$ is the positive definite matrix to be designed. g_0, g_d are the upper bound of matrix g and its first-order

derivative, respectively. To solve the problem of input saturation, the upper bound of each pair of strut angles is defined as \bar{u} , which is $u_i \in [0, \bar{u}], i = 1, 2, 3, 4$. Thus, according to Equation (11), the range control quantity in each direction is $[-\bar{u}, \bar{u}]$. Taking the y direction as an example, the relationship between the actual output $u_{y,s}$ and the desired output u_{y0} of the controller is as follows:

$$u_{y,s} = \text{sat}(u_{y0}) = \begin{cases} \bar{u}, & u_{y0} > \bar{u} \\ -\bar{u}, & u_{y0} < -\bar{u} \\ u_{y0}, & \text{else} \end{cases} \quad (17)$$

It is necessary to design an anti-windup module. Define the error between u_{y0} and $u_{y,s}$, as $\vartheta_y = u_{y0} - u_{y,s}$. From Equation (16), we know that u_{y0} is bounded, which means that ϑ_y is bounded. A fuzzy system is constructed to approximate this error as follows:

$$\vartheta_y = \theta_2^T \varphi_2 + \varepsilon_2 \quad (18)$$

Similarly, it is easy to obtain the control quantity u_{z0} in the z direction as:

$$\vartheta_z = \theta_3^T \varphi_3 + \varepsilon_3 \quad (19)$$

Then, the control law can be modified as follows:

$$u = \text{sat}\left(u_0 - [\hat{\theta}_2^T \varphi_2, \hat{\theta}_3^T \varphi_3]^T\right) \quad (20)$$

The adaptive law is designed as follows:

$$\begin{cases} \dot{\hat{\theta}}_1 = \frac{\gamma_1 z_2^T z_2 \varphi_1^T \varphi_1}{2\sigma_1^2} - \tau_1 \hat{\theta}_1 \\ \dot{\hat{\theta}}_2 = -\gamma_2 z_{2y} \varphi_2 - \tau_2 \hat{\theta}_2 \\ \dot{\hat{\theta}}_3 = -\gamma_3 z_{2z} \varphi_3 - \tau_3 \hat{\theta}_3 \\ \dot{\hat{E}} = \gamma_4 z_2^{abs} - \tau_4 \hat{E} \end{cases} \quad (21)$$

where $\gamma_1, \tau_1, \gamma_2, \tau_2, \gamma_3, \tau_3, \gamma_4, \tau_4 > 0$ are all the parameters to be designed. z_2^{abs} represents a vector consisting of the absolute values of each component of z_2 . The control law and the adaptive law, shown as (20) and (21), can maneuver the refueling drogue to a given desired position.

It is worth noting that the influence of complex environmental factors on the dynamic model of the drogue is mainly reflected in two aspects: the uncertainty of hose tension and the uncertainty of aerodynamic parameters. For hose tension uncertainty, the adaptive fuzzy system can compensate by approaching its upper bound in the controller. For the problem of uncertainty of aerodynamic parameters, the upper bound of the control gain is used in the design of the control law to effectively suppress its influence on control accuracy.

3.3. Stability Proof

The stability of the designed controller is demonstrated in this section by using Lyapunov's stability theory.

The Lyapunov function is defined as:

$$V_2 = V_1 + \frac{1}{2} z_2^T g^{-1} z_2 + \frac{1}{2\gamma_1} \tilde{\Theta}_1^2 + \frac{1}{2\gamma_2} \tilde{\theta}_2^T \tilde{\theta}_2 + \frac{1}{2\gamma_3} \tilde{\theta}_3^T \tilde{\theta}_3 + \frac{1}{2\gamma_4} \tilde{E}^T \tilde{E} \quad (22)$$

Its derivative is given by

$$\dot{V}_2 = \dot{V}_1 + z_2^T g^{-1} \dot{z}_2 - z_2^T \dot{g} g^{-2} z_2 - \frac{1}{\gamma_1} \tilde{\Theta}_1 \dot{\tilde{\Theta}}_1 - \frac{1}{\gamma_2} \tilde{\theta}_2^T \dot{\tilde{\theta}}_2 - \frac{1}{\gamma_3} \tilde{\theta}_3^T \dot{\tilde{\theta}}_3 - \frac{1}{\gamma_4} \tilde{E}^T \dot{\tilde{E}} \quad (23)$$

Equation (20) can be rewritten as:

$$\begin{aligned} \mathbf{u} &= \text{sat}\left(\mathbf{u}_0 - \begin{bmatrix} \hat{\boldsymbol{\theta}}_2^T \boldsymbol{\varphi}_2 \\ \hat{\boldsymbol{\theta}}_3^T \boldsymbol{\varphi}_3 \end{bmatrix}\right) = \mathbf{u}_0 - \mathbf{u}_0 + \text{sat}(\mathbf{u}_0) - \begin{bmatrix} \hat{\boldsymbol{\theta}}_2^T \boldsymbol{\varphi}_2 \\ \hat{\boldsymbol{\theta}}_3^T \boldsymbol{\varphi}_3 \end{bmatrix} \\ &= \mathbf{u}_0 + \begin{bmatrix} \hat{\boldsymbol{\theta}}_2^T \boldsymbol{\varphi}_2 - \vartheta_y \\ \hat{\boldsymbol{\theta}}_3^T \boldsymbol{\varphi}_3 - \vartheta_z \end{bmatrix} = \mathbf{u}_0 - \begin{bmatrix} \tilde{\boldsymbol{\theta}}_2^T \boldsymbol{\varphi}_2 - \varepsilon_2 \\ \tilde{\boldsymbol{\theta}}_3^T \boldsymbol{\varphi}_3 - \varepsilon_3 \end{bmatrix} \end{aligned} \tag{24}$$

According to the Young’s inequality [30]:

$$\mathbf{z}_2^T \tilde{\boldsymbol{\theta}}_1^T \boldsymbol{\varphi}_1 \leq \frac{\Theta_1 \mathbf{z}_2^T \mathbf{z}_2 \boldsymbol{\varphi}_1^T \boldsymbol{\varphi}_1}{2\sigma_1^2} + \frac{\sigma_1^2}{2} \tag{25}$$

Combining Equation (23), Equation (24) and Equation (25),

$$\begin{aligned} \dot{V}_2 &\leq \dot{V}_1 + \mathbf{z}_2^T \left[\frac{\Theta_1 \mathbf{z}_2^T \boldsymbol{\varphi}_1}{2\sigma_1^2} - \mathbf{g}_d \mathbf{g}_0^{-2} \mathbf{z}_2 + \mathbf{u} \right] - \frac{1}{\gamma_1} \tilde{\Theta}_1 \dot{\hat{\Theta}}_1 - \frac{1}{\gamma_2} \tilde{\boldsymbol{\theta}}_2^T \dot{\hat{\boldsymbol{\theta}}}_2 - \frac{1}{\gamma_3} \tilde{\boldsymbol{\theta}}_3^T \dot{\hat{\boldsymbol{\theta}}}_3 - \frac{1}{\gamma_4} \tilde{\mathbf{E}}^T \dot{\hat{\mathbf{E}}} + \frac{\sigma_1^2}{2} \\ &\leq -\mathbf{z}_1^T \mathbf{K}_1 \mathbf{z}_1 - \mathbf{z}_2^T \mathbf{K}_2 \mathbf{z}_2 + \mathbf{z}_2^T [\boldsymbol{\varepsilon} - \hat{\mathbf{E}} \text{sgn}(\mathbf{z}_2)] - \frac{1}{\gamma_1} \tilde{\Theta}_1 \left(\dot{\hat{\Theta}}_1 - \frac{\gamma_1 \mathbf{z}_2^T \mathbf{z}_2 \boldsymbol{\varphi}_1^T \boldsymbol{\varphi}_1}{2\sigma_1^2} \right) \\ &\quad - \frac{1}{\gamma_2} \tilde{\boldsymbol{\theta}}_2^T \left(\dot{\hat{\boldsymbol{\theta}}}_2 + \gamma_2 \mathbf{z}_2 \boldsymbol{\varphi}_2 \right) - \frac{1}{\gamma_3} \tilde{\boldsymbol{\theta}}_3^T \left(\dot{\hat{\boldsymbol{\theta}}}_3 + \gamma_3 \mathbf{z}_2 \boldsymbol{\varphi}_3 \right) - \frac{1}{\gamma_4} \tilde{\mathbf{E}}^T \dot{\hat{\mathbf{E}}} + \frac{\sigma_1^2}{2} \end{aligned} \tag{26}$$

where $\boldsymbol{\varepsilon} = (\boldsymbol{\varepsilon}_1 + [\varepsilon_2, \varepsilon_3]^T)$.

Considering that $\boldsymbol{\varepsilon}$ has an upper bound \mathbf{E} , then:

$$\mathbf{z}_2^T \boldsymbol{\varepsilon} \leq \left| \mathbf{z}_2^T \boldsymbol{\varepsilon} \right| \leq \left(\mathbf{z}_2^{abs} \right)^T \hat{\mathbf{E}} + \left(\mathbf{z}_2^{abs} \right)^T \tilde{\mathbf{E}} \tag{27}$$

Substituting Equation (27) and the adaptive law Equation (21) into Equation (26),

$$\begin{aligned} \dot{V}_2 &\leq -\mathbf{z}_1^T \mathbf{K}_1 \mathbf{z}_1 - \mathbf{z}_2^T \mathbf{K}_2 \mathbf{z}_2 - \frac{1}{\gamma_1} \tilde{\Theta}_1 \left(\dot{\hat{\Theta}}_1 - \frac{\gamma_1 \mathbf{z}_2^T \mathbf{z}_2 \boldsymbol{\varphi}_1^T \boldsymbol{\varphi}_1}{2\sigma_1^2} \right) - \frac{1}{\gamma_2} \tilde{\boldsymbol{\theta}}_2^T \left(\dot{\hat{\boldsymbol{\theta}}}_2 + \gamma_2 \mathbf{z}_2 \boldsymbol{\varphi}_2 \right) \\ &\quad - \frac{1}{\gamma_3} \tilde{\boldsymbol{\theta}}_3^T \left(\dot{\hat{\boldsymbol{\theta}}}_3 + \gamma_3 \mathbf{z}_2 \boldsymbol{\varphi}_3 \right) - \frac{1}{\gamma_4} \tilde{\mathbf{E}}^T \left(\dot{\hat{\mathbf{E}}} - \gamma_4 \mathbf{z}_2^{abs} \right) + \frac{\sigma_1^2}{2} \\ &\leq -\mathbf{z}_1^T \mathbf{K}_1 \mathbf{z}_1 - \mathbf{z}_2^T \mathbf{K}_2 \mathbf{z}_2 + \frac{\tau_1}{\gamma_1} \tilde{\Theta}_1 \dot{\hat{\Theta}} + \frac{\tau_2}{\gamma_2} \tilde{\boldsymbol{\theta}}_2^T \dot{\hat{\boldsymbol{\theta}}}_2 + \frac{\tau_3}{\gamma_3} \tilde{\boldsymbol{\theta}}_3^T \dot{\hat{\boldsymbol{\theta}}}_3 + \frac{\tau_4}{\gamma_4} \tilde{\mathbf{E}}^T \dot{\hat{\mathbf{E}}} + \frac{\sigma_1^2}{2} \end{aligned} \tag{28}$$

According to the Young’s inequality,

$$\begin{cases} \tilde{\Theta}_1 \dot{\hat{\Theta}}_1 = \tilde{\Theta}_1 \dot{\Theta}_1^* - \tilde{\Theta}_1^2 \leq \frac{1}{2} \dot{\Theta}_1^{*2} - \frac{1}{2} \tilde{\Theta}_1^2 \\ \tilde{\boldsymbol{\theta}}_2^T \dot{\hat{\boldsymbol{\theta}}}_2 = \tilde{\boldsymbol{\theta}}_2^T \dot{\boldsymbol{\theta}}_2^* - \tilde{\boldsymbol{\theta}}_2^T \tilde{\boldsymbol{\theta}}_2 \leq \frac{1}{2} \dot{\boldsymbol{\theta}}_2^{*T} \dot{\boldsymbol{\theta}}_2^* - \frac{1}{2} \tilde{\boldsymbol{\theta}}_2^T \tilde{\boldsymbol{\theta}}_2 \\ \tilde{\boldsymbol{\theta}}_3^T \dot{\hat{\boldsymbol{\theta}}}_3 = \tilde{\boldsymbol{\theta}}_3^T \dot{\boldsymbol{\theta}}_3^* - \tilde{\boldsymbol{\theta}}_3^T \tilde{\boldsymbol{\theta}}_3 \leq \frac{1}{2} \dot{\boldsymbol{\theta}}_3^{*T} \dot{\boldsymbol{\theta}}_3^* - \frac{1}{2} \tilde{\boldsymbol{\theta}}_3^T \tilde{\boldsymbol{\theta}}_3 \\ \tilde{\mathbf{E}}^T \dot{\hat{\mathbf{E}}} = \tilde{\mathbf{E}}^T \dot{\mathbf{E}}^* - \tilde{\mathbf{E}}^T \tilde{\mathbf{E}} \leq \frac{1}{2} \dot{\mathbf{E}}^{*T} \dot{\mathbf{E}}^* - \frac{1}{2} \tilde{\mathbf{E}}^T \tilde{\mathbf{E}} \end{cases} \tag{29}$$

Then, Equation (28) can be transformed into:

$$\begin{aligned} \dot{V}_2 &\leq -\mathbf{z}_1^T \mathbf{K}_1 \mathbf{z}_1 - \mathbf{z}_2^T \mathbf{K}_2 \mathbf{z}_2 - \frac{\tau_1}{2\gamma_1} \tilde{\Theta}_1^2 - \frac{\tau_2}{2\gamma_2} \tilde{\boldsymbol{\theta}}_2^T \tilde{\boldsymbol{\theta}}_2 - \frac{\tau_3}{2\gamma_3} \tilde{\boldsymbol{\theta}}_3^T \tilde{\boldsymbol{\theta}}_3 - \frac{\tau_4}{2\gamma_4} \tilde{\mathbf{E}}^T \tilde{\mathbf{E}} \\ &\quad + \frac{\tau_1}{2\gamma_1} \dot{\Theta}_1^{*2} + \frac{\tau_2}{2\gamma_2} \dot{\boldsymbol{\theta}}_2^{*T} \dot{\boldsymbol{\theta}}_2^* + \frac{\tau_3}{2\gamma_3} \dot{\boldsymbol{\theta}}_3^{*T} \dot{\boldsymbol{\theta}}_3^* + \frac{\tau_4}{2\gamma_4} \dot{\mathbf{E}}^{*T} \dot{\mathbf{E}}^* + \frac{\sigma_1^2}{2} \\ &= -\rho_1 V_2 + \rho_2 \end{aligned} \tag{30}$$

where $\rho_1 = 2\min\{\lambda_{\min}(\mathbf{K}_1), \lambda_{\min}(\mathbf{K}_2 \mathbf{g}_0), \tau_1, \tau_2, \tau_3, \tau_4\}$

$$\rho_2 = \frac{\tau_1}{2\gamma_1} \dot{\Theta}_1^{*2} + \frac{\tau_2}{2\gamma_2} \dot{\boldsymbol{\theta}}_2^{*T} \dot{\boldsymbol{\theta}}_2^* + \frac{\tau_3}{2\gamma_3} \dot{\boldsymbol{\theta}}_3^{*T} \dot{\boldsymbol{\theta}}_3^* + \frac{\tau_4}{2\gamma_4} \dot{\mathbf{E}}^{*T} \dot{\mathbf{E}}^* + \frac{\sigma_1^2}{2}.$$

Integrating Equation (30), we obtain:

$$V_2 \leq V_2(0)e^{-\rho_1 t} + \rho_2 / \rho_1 \tag{31}$$

It is proved that the controller and adaptive laws designed in this paper can make z_1 , z_2 , $\tilde{\Theta}_1$, $\tilde{\theta}_2$, $\tilde{\theta}_3$ and \tilde{E} uniformly ultimately bounded [31], whose bound ρ_1/ρ_2 can come to be arbitrarily small by the parameter adjustment of ρ_1 and ρ_2 . This ends the proof.

4. Discussion

This section verifies the controller's capability of handling model uncertainties and disturbances, as well as tracking continuous trajectory instruction. Parameters of the refueling hose and the drogue are shown as follows [15]: The initial length of the hose is 30 m. The hose diameter is 0.05 m. The hose linear density is 0.48 kg/m. The hose skin friction coefficient is 0.01, and the crossflow coefficient is 0.5. The initial number of links in the dynamic model was chosen as 5. The characteristic area and length of the drogue are 0.3 square meters and 0.25 m. The drogue mass is 20 kg. The inertia moment of the drogue is 7.99 kg · m², 4.44 kg · m² and 4.44 kg · m² in the directions of x, y, z . The tanker flew in a straight line at a constant speed, flying at an altitude of 7000 m and a speed of 200 m/s. Nominal aerodynamic force and moment parameters of the drogue are shown as follows. Aerodynamic parameters are obtained from the wind tunnel tests shown in reference [32].

$$C_{Ddro}^u = \begin{bmatrix} -0.151 & -0.151 & -0.151 & -0.151 \\ -0.0093 & 0 & 0.0093 & 0 \\ 0 & -0.0093 & 0 & -0.0093 \end{bmatrix}$$

$$C_{Ddro}^{\alpha,\beta} = \begin{bmatrix} 4.632 - 0.00055\alpha^2 - 0.00055\beta^2 \\ -0.0148\beta \\ 0.0148\alpha \end{bmatrix}$$

$$C_{Mdro}^u = \begin{bmatrix} 0 & 0 & 0 & 0 \\ 0 & -0.0054 & 0 & 0.0054 \\ -0.0054 & 0 & 0.0054 & 0 \end{bmatrix}$$

$$C_{Mdro}^{\alpha,\beta} = \begin{bmatrix} 0 \\ -0.0816\alpha \\ -0.0816\beta \end{bmatrix}$$

The controller parameters were chosen as: $K_1 = \text{diag}(20, 20)$, $K_2 = \text{diag}(0.01, 0.01)$, $\sigma = 1$, $\gamma_1 = 10$, $\tau_1 = 0.001$, $\gamma_2 = 1$, $\tau_2 = 1$, $\gamma_3 = 1$, $\tau_3 = 1$, $\gamma_4 = 10$, $\tau_4 = 20$, $\sigma_1^2 = 100$, where K_1 and K_2 have a direct effect on the system's convergence rate and features. Furthermore, γ_1 and τ_1 have a clear influence on the results, while other parameters are insensitive to the results. The steady-state inaccuracy is reduced as γ_1 decreases, while the oscillation amplitude increases. And increasing τ_1 can accelerate convergence but degrade steady-state performance. The membership function of the fuzzy system is chosen as Gaussian type, i.e., $\mu_i = \exp\left(-\frac{(X_i - b_i)^2}{\sigma_{fuzzy}^2}\right)$, where $X = [x_d^T, \dot{x}_d^T, u^T, v_n, \vartheta_{1i}, \vartheta_{2i}]^T$ is the input variable of the fuzzy system, $\sigma_{fuzzy} = 50$ and $b_i = [-15, -14, \dots, -1, 0, 1, \dots, 14, 15]_{1 \times 31}$.

In order to verify the anti-disturbance capability, the complex flow field, which consists of a tanker trail vortex, atmospheric turbulence, receiver bow wave and wind gust is considered [33]. The first three items are modeled in the reference by [34]. The gust is modeled using the "1-cosine" full wavelength model starting from the 20th second and lasting 13 s with an amplitude of 20 m/s in directions of x, y . Furthermore, according to the analysis in Section 3, the uncertainty of the drogue's aerodynamic parameters is closely related to the wind disturbance, which also needs to be considered in this section. For the sake of simplicity, it is assumed that the drogue's aerodynamic parameters change with wind speed, with the maximum change being 250% of the nominal value. The variation in wind disturbance and the drogue's aerodynamic parameters are shown in Figure 5.

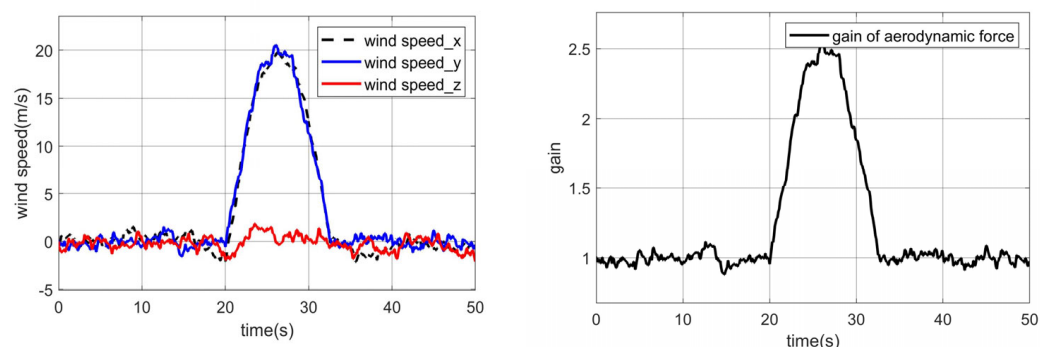


Figure 5. Variation in wind disturbance (left) and the drogue's aerodynamic parameters (right).

In order to verify the effectiveness of the proposed controller, the following two sets of simulation experiments were designed.

Simulation I: Experiment for handling the disturbances and uncertainties. This simulation takes into account both complex flow fields and uncertainty in aerodynamic parameters. The aim is that the drogue moves to the fixed desired position $[-28, 4, 5]$ m from the initial position $[-30, 0, 0]$ m and remains stable. Under the control framework of this paper, comparative tests were designed, respectively:

Controller A represents the cooperative controller designed in this paper.

Controller B represents the traditional back-stepping controller.

Controller C represents the adaptive fuzzy controller without the technology of error estimation.

Figure 6 (left) depicts the drogue position when three controllers are used. Under the action of controller A and controller C, the position of the drogue can be rapidly converged. Controller A presented in this paper has better convergence characteristics and can reach the desired position within 1 s, while controller C requires 4 s. Furthermore, when the gust and aerodynamic parameter change occurred at the 20th second, the position changes in the three directions under controller B were 0.28 m, 0.9 m and 0.75 m, respectively. This is because the uncertainty of aerodynamic parameters has a great influence on the accuracy of classical back-stepping control, which is consistent with the theoretical analysis. These changes were reduced to 0.002 m, 0.006 m and 0.009 m under controller A and controller C. Therefore, it shows that the controller presented in this paper has better convergence speed and steady-state performance and can effectively suppress the influence of uncertainty in aerodynamic parameters. Figure 6 (right) shows the variation in the hose length and angles of the drogue struts u_y, u_z , respectively. The angles of struts have always been within the interval of $[-\bar{u}, \bar{u}]$, which means that the cooperative controller proposed in this paper can achieve stable control of the drogue while satisfying the input constraints.

Remark: It can be noted that the maneuverability range of the drogue reaches up to 6 m. However, the maneuvering distance achieved through the sole use of the drogue is less than 2 m, which proves the effectiveness of the collaborative control framework.

Figure 7 (left) shows the variation in the hose attitude. As mentioned above, the hose recovery moment has a significant influence on the drogue, causing the attitude to tend to be stable with positions becoming stable. In addition, when the aerodynamic moment parameters of the drogue change, the attitude of the drogue is changed by no more than $0.1\text{rad}(5.73^\circ)$. Figure 7 (right) shows the variation in the upper bound of ε , which converges to near 0 within 2 s. This result shows that the fuzzy systems designed above could quickly approximate the model uncertainties, as well as the error between the actual and ideal output of the actuators, and maintain stability with a small error.

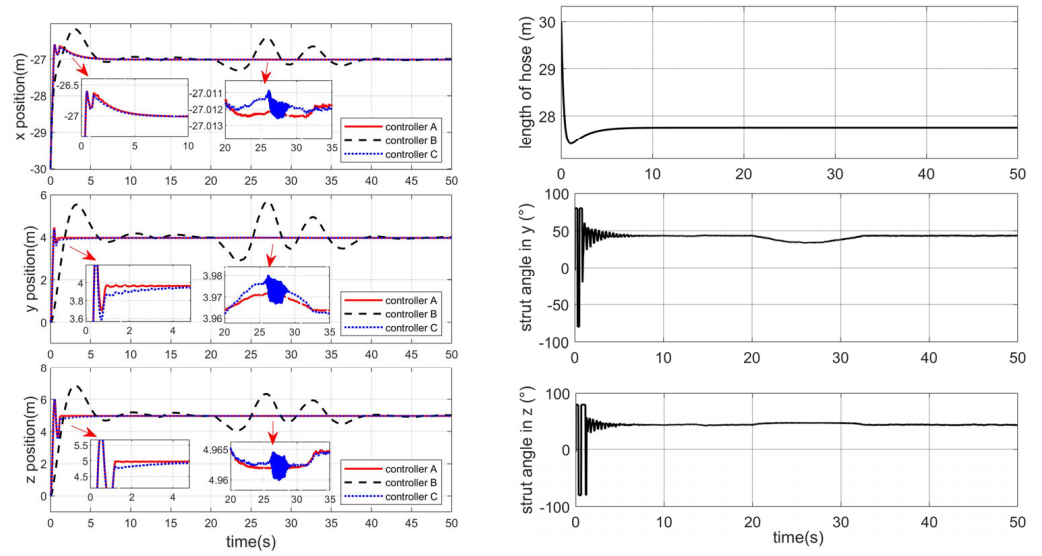


Figure 6. Drogue positions (left) and hose length and strut angles (right) in simulation I.

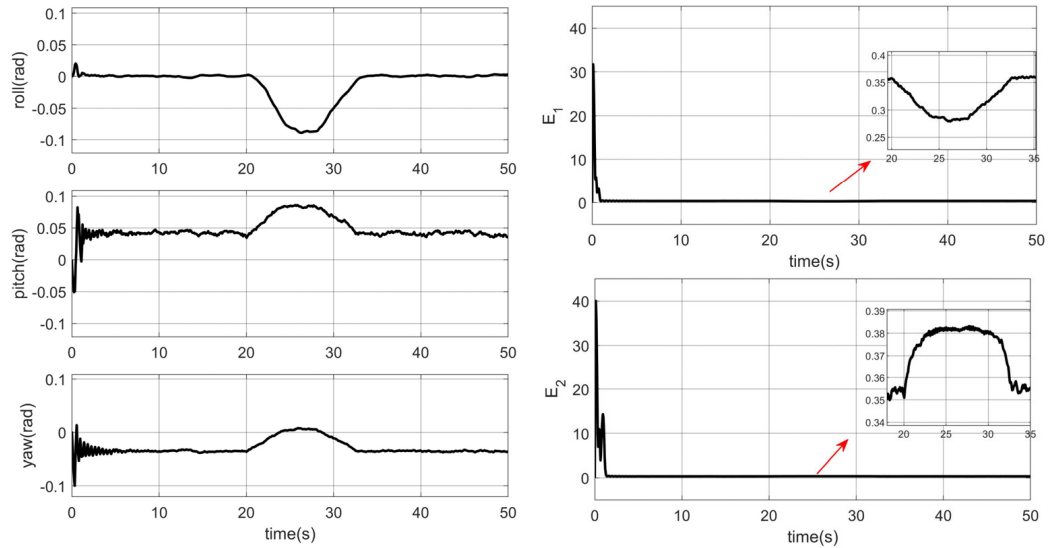


Figure 7. Drogue attitude (left) and upper bound of ϵ (right) in simulation I.

Simulation II: Experiment for continuous trajectory tracking. The desired position instruction of the drogue is not fixed in actual aerial refueling missions but is provided by the outer ring guidance loop, which is generally a continuous signal. The simulation experiment is designed as follows to test the drogue’s ability to track the continuous desired position instruction: under the influence of a complex flow field and uncertainty of aerodynamic parameters, the initial position of the drogue is $[-30, 0, 0]$ m, and the desired trajectory instruction is:

$$\begin{cases} x_d = 4 \sin(0.5t) - 26 \text{ (m)} \\ y_d = 2 \sin(0.2t) + 3 \text{ (m)} \\ z_d = \sin(0.5t + \pi/2) + 2 \text{ (m)} \end{cases} \quad (32)$$

The simulation results are shown in Figure 8. The results show that the desired trajectory is tracked well in all three directions. The maximum tracking error in both y, z directions is 0.1 m and 0.05 m, respectively, which meets the requirements of the air refueling mission. The x direction tracking effect is slightly worse, with a maximum error of 0.22 m. As discussed in Section 3, the accuracy requirement in the x direction is far less than in the

other two directions. The designed cooperative controller can make the drogue track the continuous trajectory command well and meet the requirements of AAR. In Figure 8 (right), we can find that the actual input of actuators has always satisfied the input constraints.

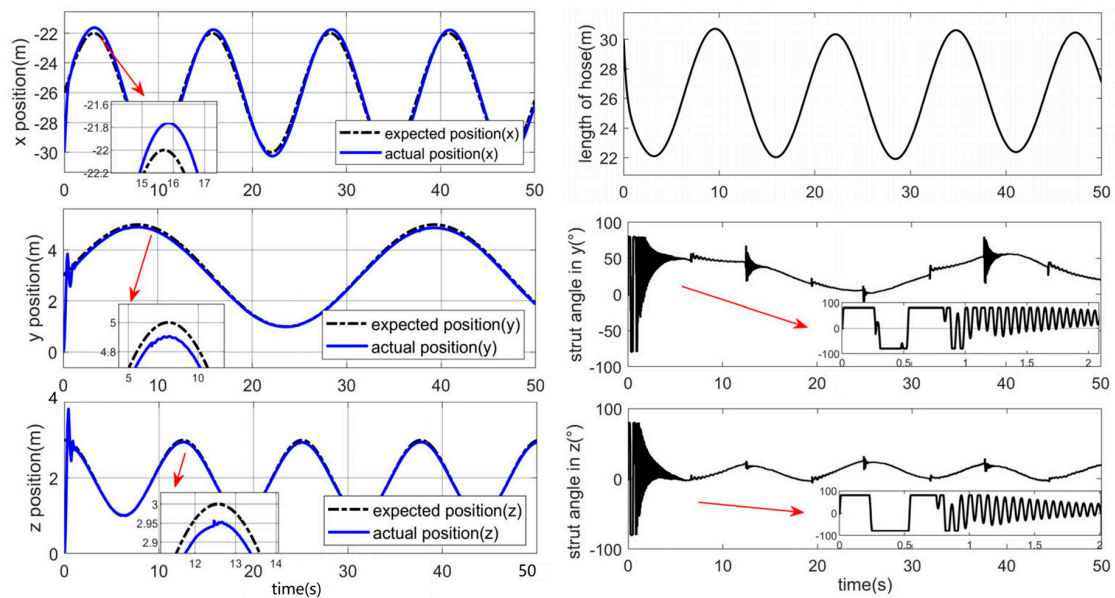


Figure 8. Drogue positions (left) and hose length and strut angles (right) in simulation II.

5. Conclusions

To achieve wide-range maneuverability control for the controllable drogue, this paper proposes a cooperative control framework, which includes an open-loop control of the hose based on neural networks and a closed-loop control of the drogue based on fuzzy approximation. The primary adjusting parameters K_1 , K_2 , γ_1 and τ_1 can provide an effective control effect. Simulation results indicate that the proposed scheme, as compared to the maneuvering scheme relying solely on the drogue, enables a wider range of maneuverability and exhibits superior performance in handling issues such as modeling inaccuracies and uncertainties in aerodynamic parameters. However, the current study contains the following limitations: 1. Open-loop control has low accuracy while dealing with problems like sensor errors and actuator breakdowns. 2. Offline-trained GRUs have insufficient accuracy when dealing with non-involved samples. To solve the aforementioned issues, the authors intend to develop closed-loop control based on online-trained GRUs, and then design an asynchronous full closed-loop control framework by merging the drogue's high-precision closed-loop control method.

Author Contributions: Z.M.: conceptualization, resources, writing—review and editing, supervision, project administration and funding acquisition. J.B.: methodology, software, investigation, data curation, validation, writing—original draft, and visualization. All authors have read and agreed to the published version of the manuscript.

Funding: This research is supported by the National Natural Science Foundation of China (Grant No: 62173273).

Data Availability Statement: The data used in the experiments are available in the paper.

Conflicts of Interest: The authors declare no conflicts of interest.

References

1. Park, C.; Ramirez-Serrano, A.; Bisheban, M. Adaptive Incremental Nonlinear Dynamic Inversion Control for Aerial Manipulators. *Aerospace* **2024**, *11*, 671. [[CrossRef](#)]
2. Lin, P.; He, Y.; Cen, Y. Unmanned autonomous air-to-air refueling intelligent docking technology. *Chin. J. Aeronaut.* **2024**, *37*, 1–5. [[CrossRef](#)]

3. Chen, D.; Xu, L.; Wang, C. An Advanced Control Method for Aircraft Carrier Landing of UAV Based on CAPF–NMPC. *Aerospace* **2024**, *11*, 656. [[CrossRef](#)]
4. Zheng, C.; Wang, H.; Hu, L.; Cai, Y. Research on the Motion and Dynamic Characteristics of the Hose-and-Drogue System under Bow Wave. *Aerospace* **2024**, *11*, 13. [[CrossRef](#)]
5. Williamson, W.R.; Reed, E.; Glenn, G.J.; Stecko, S.M.; Musgrave, J.; Takacs, J.M. Controllable Drogue for Automated Aerial Refueling. *J. Aircraft* **2010**, *47*, 515–527. [[CrossRef](#)]
6. Duan, H.; Sun, Y.; Shi, Y. Bionic Visual Control for Probe-and-Drogue Autonomous Aerial Refueling. *IEEE Trans. Aerosp. Electron. Syst.* **2021**, *57*, 848–865. [[CrossRef](#)]
7. Ro, K.; Kuk, T.; Kamman, J.W. Dynamics and Control of Hose-Drogue Refueling Systems During Coupling. *J. Guid. Control Dyn.* **2011**, *34*, 1694–1708. [[CrossRef](#)]
8. Fezans, N.; Jann, T. Modeling and Simulation for the Automation of Aerial Refueling of Military Transport Aircraft with the Probe-and-Drogue System. In Proceedings of the AIAA Modeling and Simulation Technologies Conference, Denver, CO, USA, 5–9 June 2017.
9. Paniagua, K.S.; Garcia-Fogeda, P.; Arevalo, F.; Rodriguez, J.B. Aeroelastic analysis of an air-to-air refueling hose-drogue system through an efficient novel mathematical model. *J. Fluid. Struct.* **2021**, *100*, 103164.
10. Ro, K.; Kamman, J.W. Modeling and Simulation of Hose-Paradrogue Aerial Refueling Systems. *J. Guid. Control Dyn.* **2010**, *33*, 53–63. [[CrossRef](#)]
11. Wang, H.; Dong, X.; Liu, J.; Wang, J. Dynamics and control of the hose whipping phenomenon in aerial refueling. In Proceedings of the 2015 IEEE Aerospace Conference, IEEE, Big Sky, MT, USA, 7–14 March 2015; pp. 1–18.
12. Clifton, J.M.; Schmidt, L.V.; Stuart, T.D. Dynamic modeling of a trailing wire towed by an orbiting aircraft. *J. Guid. Control Dyn.* **1995**, *18*, 875–881. [[CrossRef](#)]
13. Kamman, J.W.; Huston, R.L. Multibody dynamics modeling of variable length cable systems. *Multibody Syst. Dyn.* **2001**, *5*, 211–221. [[CrossRef](#)]
14. Cheng, J.; Ji, K. Dynamic modeling and simulation of variable-length hose–drogue aerial refueling systems. *AIP Adv.* **2022**, *12*, 015104. [[CrossRef](#)]
15. Su, Z.; Li, C.; Liu, Y. Anti-disturbance dynamic surface trajectory stabilization for the towed aerial recovery drogue under unknown airflow disturbances. *Mech. Syst. Signal Proc.* **2021**, *150*, 107342. [[CrossRef](#)]
16. Su, Z.; Li, C.; Wu, J.; Wang, H. Neuro-Adaptive Prescribed Performance Control for Aerial-Recovery Drogue with Actuator Constraints. *J. Guid. Control Dyn.* **2022**, *45*, 1451–1465. [[CrossRef](#)]
17. Liu, Z.; Liu, J.; He, W. Dynamic modeling and vibration control of a flexible aerial refueling hose. *Aerosp. Sci. Technol.* **2016**, *55*, 92–102. [[CrossRef](#)]
18. Liu, Z.; Liang, J.; Zhao, Z.; Efe, M.O.; Hong, K. Adaptive Fault-Tolerant Control of a Probe-and-Drogue Refueling Hose Under Varying Length and Constrained Output. *IEEE Trans. Control Syst. Technol.* **2022**, *30*, 869–876. [[CrossRef](#)]
19. Liu, Z.; Han, Z.; He, W. Adaptive Fault-Tolerant Boundary Control of an Autonomous Aerial Refueling Hose System with Prescribed Constraints. *IEEE Trans. Autom. Sci. Eng.* **2022**, *19*, 2678–2688. [[CrossRef](#)]
20. Song, M.; Zhang, F.; Huang, B.; Huang, P. Anti-Disturbance Control for Tethered Aircraft System With Deferred Output Constraints. *IEEE/CAA J. Autom. Sinica.* **2023**, *10*, 474–485. [[CrossRef](#)]
21. Chen, L.; Liang, H.; Pan, Y.; Li, T. Human-in-the-loop consensus tracking control for UAV systems via an improved prescribed performance approach. *IEEE Trans. Aerosp. Electron. Syst.* **2023**, *59*, 8380–8391. [[CrossRef](#)]
22. Pan, Y.; Ji, W.; Lam, H.-K.; Cao, L. An improved predefined-time adaptive neural control approach for nonlinear multiagent systems. *IEEE Trans. Autom. Sci. Eng.* **2023**, 1–10, early access. [[CrossRef](#)]
23. Campos-Martinez, S.N.; Hernandez-Gonzalez, O.; Guerrero-Sanchez, M.E.; Valencia-Palomo, G.; Targui, B.; Lopez-Estrada, F.R. Consensus Tracking Control of Multiple Unmanned Aerial Vehicles Subject to Distinct Unknown Delays. *Machines* **2024**, *12*, 337. [[CrossRef](#)]
24. Bianchi, D.; Di Gennaro, S.; Di Ferdinando, M.; Lua, C.A. Robust Control of UAV with Disturbances and Uncertainty Estimation. *Machines* **2023**, *11*, 352. [[CrossRef](#)]
25. Yang, S.; Zou, Z.; Li, Y.; Shi, H.; Fu, Q. Adaptive Fault-Tolerant Tracking Control of Quadrotor UAVs against Uncertainties of Inertial Matrices and State Constraints. *Drones* **2023**, *7*, 107. [[CrossRef](#)]
26. Zhu, G.; Lv, L.; Sun, L.; Zhang, X. Distributed Dynamic Surface Control for a Class of Quadrotor UAVs with Input Saturation and External Disturbance. *Drones* **2024**, *8*, 77. [[CrossRef](#)]
27. Cai, J.; Mei, C.; Yan, Q. Semi-global adaptive backstepping control for parametric strict-feedback systems with non-triangular structural uncertainties. *ISA Trans.* **2022**, *126*, 180–189. [[CrossRef](#)]
28. Song, M.; Huang, P. Dynamics and Anti-Disturbance Tracking Control for Tethered Aircraft System. *Nonlinear Dynamics.* **2022**, *110*, 2383–2399. [[CrossRef](#)]
29. Sun, W.; Su, S.-F.; Xia, J.; Nguyen, V.-T. Adaptive Fuzzy Tracking Control of Flexible-Joint Robots With Full-State Constraints. *IEEE Trans. Syst. Man Cybern. Systems* **2019**, *49*, 2201–2209. [[CrossRef](#)]
30. Wang, H.; Liu, P.X.; Xie, X.; Liu, X.; Hayat, T.; Alsaadi, F.E. Adaptive fuzzy asymptotical tracking control of nonlinear systems with unmodeled dynamics and quantized actuator. *Inf. Sci.* **2021**, *575*, 779–792. [[CrossRef](#)]

31. Lai, G.; Liu, Z.; Zhang, Y.; Chen, X.; Chen, C.L.P. Robust Adaptive Fuzzy Control of Nonlinear Systems with Unknown and Time-Varying Saturation. *Asian J. Control* **2015**, *17*, 791–805. [[CrossRef](#)]
32. Meng, Z.; Bai, J.; Yan, B.; Li, S. An Autonomous Aerial Refueling Controllable Drogue with Adjustable Strut Angle: Control and Test. *IEEE/ASME Trans. Mechatron* **2023**, 1–11, *early access*. [[CrossRef](#)]
33. Rena, J.; Quan, Q. Progress in modeling and control of probe-and-drogue autonomous aerial refueling. *Chin. J. Aeronaut.* **2024**, *37*, 6–26. [[CrossRef](#)]
34. Dai, X.; Wei, Z.; Quan, Q. Modeling and simulation of bow wave effect in probe and drogue aerial refueling. *Chin. J. Aeronaut.* **2016**, *29*, 448–461. [[CrossRef](#)]

Disclaimer/Publisher’s Note: The statements, opinions and data contained in all publications are solely those of the individual author(s) and contributor(s) and not of MDPI and/or the editor(s). MDPI and/or the editor(s) disclaim responsibility for any injury to people or property resulting from any ideas, methods, instructions or products referred to in the content.